Journal of Rehabilitation in Civil Engineering 7-3 (2019) 117-138

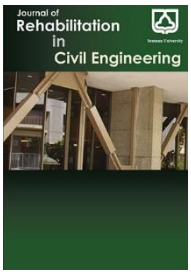

Journal homepage: http://civiljournal.semnan.ac.ir/

Experimental Investigation of Corrosion Cracking in Reinforced Concrete Beams Containing Nano Wollastonite

M. Miri[1*], M. Reza Ghasemi[2] and H. Beheshti Nezhad[3]

1. Professor, Civil Engineering Department, University of Sistan and Baluchestan, Zahedan, Iran
2. Professor, Civil Engineering Departmnent, University of Sistan and Baluchestan, Zahedan, Iran
3. Department of Civil Engineering, Birjand Branch, Islamic Azad University, Birjand, Iran

Corresponding author: *mmiri@eng.usb.ac.ir*

ARTICLE INFO

Article history:
Received: 23 December 2017
Accepted: 14 July 2018

Keywords:
Reinforced Concrete Beam,
Corrosion,
Crack,
Nano Wollastonite,
GMDH-type Neural Network.

ABSTRACT

Cracking of the concrete cover due to corrosion is defined as the serviceability limit state of reinforced concrete structures. This study evaluated the influence of a mineral admixture i.e. nano wollastonite on corrosion performance and serviceability of reinforced concrete structures by performing an accelerated corrosion test on ten reinforced concrete beams under a sustained load. To do so, five concrete beams were treated with nano wollastonite (NCW), while the others were normal concrete beams (NC). The results were discussed in terms of corrosion crack patterns, crack width, half-cell potentials, rebar mass loss, and rebar diameter degradation at different corrosion levels. The results showed that the incorporation of nano wollastonite in reinforced concrete beams increased the service life by increasing the initial cracking time, decreasing the corrosion crack growth rate and rebar mass loss. Given the maximum 0.3 mm corrosion crack width as limit state criteria, the lifetime of the NCW reinforced beams was 3.6 times longer than that of Group NC. The experimental results were compared with existing models. However, these models were unreliable in predicting the steel cross-section loss based on crack width. To solve this problem, a GMDH-type neural network model was developed and evaluated using obtained experimental data for NC and NCW beams.

1. Introduction

Corrosion of reinforcing bars in concrete is one of the most prominent causes of the deterioration of reinforced concrete structures [1]. When concrete is subjected to a chloride-rich environment, chloride ions can penetrate and diffuse through it, finally

DOI: 10.22075/JRCE.2018.13485.1246

reaching the reinforcing bars and causing corrosion [2]. When corrosion of reinforced concrete structures occurs, the metallic iron transforms into oxide. Depending on the oxidation state, the volume of iron oxide can reach up to 600% of the volume of the original iron [3]. The tensile stresses due to the expanded corrosion products can cause cracking and spalling of the cover concrete [4].

The subsequent reduction in the effective cross-sectional area of concrete members, reduction in bond strength between the concrete and steel bars, and also losses in the cross-section of corroded steel bars will, in time, adversely affect the serviceability and strength of the RC elements.

Different treatment techniques have been used over the past decades to increase the long-term strength and durability properties. One of the most common techniques is the use of mineral admixtures as a partial replacement for cement in concrete mixtures [5-8]. Use of minerals such as silica fume, fly ash, and metakaolin as admixtures have been found to significantly improve the durability of concrete by modifying and refining concrete pore structure and as a result, restrict the movement of moisture in its pores and also increase the corrosion initiation time [9-11]. Using an admixture with fiber structure in concrete, in addition to increasing the corrosion initiation time, can reduce the cracks width expansion and thus improves the corrosion parameters. In this way, the service life of the reinforced concrete structures will be increased by considering the failure criterion in corrosion propagation period.

One of the minerals that has recently been used as fiber material in concrete is wollastonite with acicular structure. Wollastonite is calcium meta silicate and a natural, inert, acicular, white silicate mineral of high modulus of elasticity, with particle size mostly in the range of the cement particles [9-12]. It is formed as a result of the interaction of limestone with silica in hot magmas [9-12]. Ni et al. [13] investigated the possible effects of wollastonite on strength behavior of specimens of concrete. In their study, concrete mixes with cement replaced by 15% wollastonite were used to prepare flexural and compressive specimens. Results indicated improvements up to 30% and 10% in flexural and compressive strengths of concrete specimens, respectively. Kala et al. [14] investigated durability properties of concrete containing wollastonite. They observed that incorporation of wollastonite in the range of 10 -15% improved concrete's strength and durability. The porosity of concrete was reduced and its microstructure was densified by replacing cement with wollastonite in this range. The partial substitution of cement with wollastonite will also help to reduce the environmental pollution, energy demand, and production cost. The influence of wollastonite in ultra-high performance concrete, on the early-age shrinkage behavior and cracking potential was investigated by Soliman and Nehdi [15]. It was observed that adding wollastonite micro fibers led to lower mass loss and less shrinkage due to drying of the concrete specimens. Similar observations were reported by Zhang [16] and Miri et al. [12]. Results by Miri et al. [12] also indicated a water permeability decrease up to 50% when cement was replaced by 10% nano wollastonite.

They examined relatively small samples in their studies which may not reflect the in situ durability and performance of large structural

elements properly. Furthermore, results of previous works on evaluating the use of wollastonite as an admixture on reinforced concrete properties showed it had a considerable impact on strength, durability, and permeability. However, their studies did not involve the durability of specimens containing wollastonite in terms of corrosion performance, corrosion propagation, and cracking.

Researchers use the appearance of visible cracks as an indication to provide appropriate solutions. Corrosion cracking develops longitudinally throughout the steel bars and looks different from the cracking caused by bending stress, which is frequently perpendicular to the bars [3]. This so-called corrosive cracking in reinforced concrete elements, which is used as a criterion for service life, has a significant influence on the durability of reinforced concrete structures [17]. Visual inspection is the most popular technique for assessing structure degradation and drawing maps of corrosion cracks. Rebar cross-section loss is predictable using the crack width results, and thus the residual strength of the reinforced concrete member can be determined [18-22]. Few experimental works have attempted to establish a relationship between crack width and corrosion. Rodriguez et al. [19] suggested a relationship between corrosion and crack width. They used electrically accelerated methods to produce corrosion. Vidal et al. [20] studied corroded beams that had been subjected to an aggressive saline environment in wetting-drying cycles under sustained loading. They proposed a model to relate the crack width with the cross-section loss of the steel reinforcement. Zhang et al. [21] also proposed a model to relate the crack width with average mass loss of steel reinforcement. Khan et al. [22] presented a model by modifying the Zhang equation to predict rebar diameter loss according to crack width, rebar diameter, and concrete cover. In most existing models, the synergistic effect of simultaneous sustained loading and corrosion are ignored. In recent years, more studies have considered the combined effects of service loads and reinforcement corrosion on the deterioration process and rebars mass loss of RC members [4, 23-25]. Malumbela et al. [25] and Ye et al. [24] demonstrated that the maximum rebar mass loss due to corrosion happen in the middle span, in the maximum moment region of beams. Use of a reliable NDT method, such as half-cell potential (HCP), to evaluate the degradation of beams due to corrosion along with the measured crack width data for prediction of rebars mass loss can lead to accurate results. Half-cell potential (HCP), as an NDT method, has been widely used due to its reasonable field application and definite criteria for service life [1, 26]. In this method, based on [27], a high impedance voltmeter is used to measure the potential difference existing between an external electrode found on the surface of the concrete and the embedded rebar in RC structures [1]. Over the past decades, HCP has been used in field and lab experiments to evaluate the corrosion level of steel-embedded concrete [28].

The present investigation aims to determine the influence of wollastonite with fiber structure as a partial replacement of cement in nanoscale on the properties of concrete beams. Crack width, crack patterns, half-cell potential, mass loss, and rebar diameter reduction were evaluated. The experimental data were compared with existing models relating crack width to mass loss of steel cross-section. In order to investigate the synergistic effect of simultaneous sustained

loading and corrosion process on reducing the diameter of the bars in the reinforced concrete beams, the corrosion test was carried out using an accelerated corrosion test, in which the concrete beams were under sustained load. The other objective of this research is to determine the increase of concrete structures service life as a result of using nano wollastonite in their concrete mix design. Evaluation of specimens was conducted by measuring crack width as serviceability criteria.

In the last part of this study, after investigating corrosion parameters in corroded beams, a GS-GMDH type neural network model [29] was trained to predict the rebar diameter reduction based on input parameters which involved corrosion crack width, ratio moment value, and decrease values of the half-cell potential.

2. Materials and Methods

Monitoring corrosion cracking in reinforced concrete structures as a service lifetime criterion is important for determining the repair time; consequently, it can prevent the premature failure of structures.

This paper presents a test series designed to study the corrosion-induced cracking as a serviceability limit state criterion in semi-scale NCW beams compared to representative NC beams. All ten beams were corroded under a sustained load. The overall experimental program involved testing ten RC beams (1500×150×100 mm). Beams were tested under five different levels of corrosion: 2%, 5%, 10%, 15%, and 25%. Target corrosion levels were calculated using theoretical Faraday equation. According to related studies [23-25, 30-31], one beam specimen was tested for each mix design and corrosion level. All mixes in NCW group contained 10% nano wollastonite. Table 1 summarizes the experimental program.

Specimens of group NC: NC-1, NC-2, NC-3, NC-4, and NC-5 were subjected to 12, 32, 58, 85, and 142 days of corrosion exposure, respectively, without nano wollastonite. Specimens of group NCW: NCW-1, NCW-2, NCW-3, NCW-4, and NCW-5 were subjected to the same corrosion exposure as specimens of group NC, respectively, but with nano wollastonite contained in their mix design.

Table 1. Test matrix.

Group	Specimen	Time of corrosion exposure (days)	Target Corrosion Level*
NC	NC-1	12	2
	NC-2	32	5
	NC-3	58	10
	NC-4	85	15
	NC-5	142	25
NCW	NCW-1	12	2
	NCW-2	32	5
	NCW-3	58	10
	NCW-4	85	15
	NCW-5	142	25

* Calculated by theoretical equation

2.1. Details of Beam Specimens

The flexural reinforcement steel contained two 12 mm diameter rib bars (ϕ12) at the bottom and two 8 mm diameter rib bars (ϕ8) at the top. The tensile bar cover was 20 mm. The shear reinforcement contained 5 mm-diameter plain stirrups (ø5) spaced at 70 mm on center (o/c) in the shear span and at 116 mm o/c in the constant moment region. All stirrups in each specimen were insulated with epoxy glue. Moreover, PVC tape was wrapped around the stirrups corners at the contact points between the longitudinal steel bars and stirrups to avoid sharing current.

Table 2. Chemical properties of cement.

Component	SiO_2	Al_2O_3	Fe_2O_3	CaO	MgO	SO_3	Na_2O	K_2O	L.o.I
%	22.39	4.31	3.40	63.56	2.95	1.83	-	-	0.92

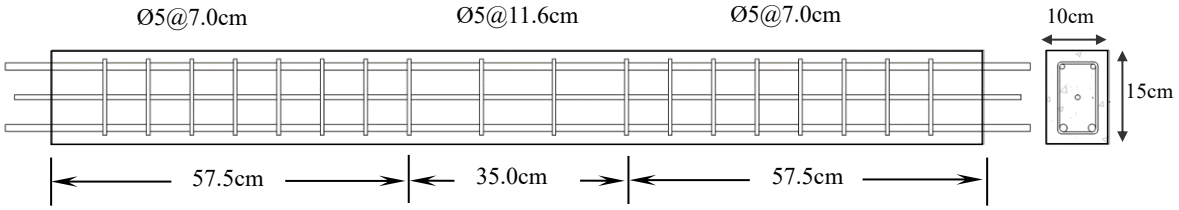

Fig. 1. Dimensions and reinforcement details of the concrete test beams.

A stainless steel bar with 8 mm diameter was placed inside the test specimen as shown in Fig. 1. The tensile reinforcement bars and stainless steel bar were extended approximately 50 mm for a suitable electrical connection. To remove any corrosion product from the surface, the steel bars were cleaned with a wire brush just before casting the reinforced specimens. NC and NCW mixes were similar in terms of materials used but specimens of group NCW contained 10% nano wollastonite.

2.2. Materials

In this study, ordinary Portland cement (ASTM C150) [32] type II with Blaine fineness (specific surface) equal to 2950 cm^2/gr were used for both NC and NCW mixtures. The chemical composition of cement is illustrated in Table 2. Fig. 2 presents the structure of nano wollastonite used in mix design of NCW specimens. According to recent researches, nano-concrete is defined as a concrete made using Portland cement and cementitious particles which fall below 500 nm [33-34].

Fig. 2. TEM micrograph of wollastonite particles.

The nano wollastonite used in this study had a fiber structure with a width between about 100 and 500 nm. The chemical composition of nano wollastonite is shown in Table 3.

Based on ASTMC618 (ASTM 2008 b) [35] wollastonite is classified as Class C pozzolan.

Natural sand with a 4.75 mm maximum size was used as a fine aggregate. Fineness modulus, special gravity, and adsorption of the fine aggregate were 3, 2.57 gr/cm^3, and 1.5%, respectively.

Table 3. Chemical properties of nano wollastonite.

Component	SiO_2	Al_2O_3	Fe_2O_3	TiO_2	CaO	MgO	Na_2O	K_2O	SO_3	L.o.I
%	46.96	3.95	2.79	0.22	39.77	1.39	0.16	0.04	0.05	4.31

Table 4. Mixture proportions for NC and NCW mixtures.

Concrete type	Cement (Kg/m^3)	Water (Kg/m^3)	Fine aggregate (Kg/m^3)	Coarse aggregate (Kg/m^3)	Nano wollastonite (Kg/m^3)
NC	400	180	943	695	–
NCW	360	180	943	695	40

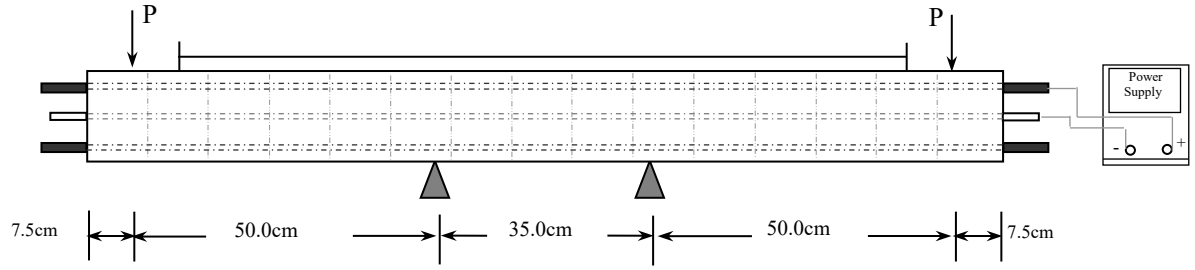

Fig. 3. Test rig for reinforcement corrosion.

Aggregates with the maximum size of 12.7 mm were used in the concrete mix with the special gravity of $2.52gr/cm^3$. Coarse and Fine aggregate gradation conformed ASTM C33 [36] limits. SPA Plast 403, naphthalene-based superplasticizer, as mentioned in ASTM C494/C494M-10 [37], was used in the concrete mixes. For obtaining the same slump in NC and NCW mixtures (5cm), the superplasticizer content of each mix was determined.

The mixture proportions for NC and NCW are summarized in Table 4. The 28-day compressive strength was, on average, 372 kg/cm^2 and $403kg/cm^2$ for the NC and NCW mixtures. The content of the binder (cement + nano wollastonite) was constant and equal to 0.45. In NCW mixture, 10% nano wollastonite was used as a replacement for cement. Type S400 and S240 steels were used as longitudinal and stirrups bars, respectively.

2.3. Casting Beam Specimens

Ten beams with two mixes as shown in Table 4 were molded and prepared for the accelerated corrosion test. The traditional slump test was applied to determine the workability of mixtures according to ASTM C 143 [38]. Cubic samples (150 × 150 × 150 mm) were prepared to determine the compressive strength according to BS 1881-116-83 [39]. The beams were de-molded after 24 hours and then cured in 100% humidity until the testing time.

2.4. Corrosion Process

After 28 days after de-molding the beams, the accelerated corrosion process was induced by impressing an average constant direct current of 164 $\mu A/cm^2$ on the tensile steel bars. According to [40], total impressed current densities were limited to $200\mu A/cm^2$.

Also, according to [41], the corrosion process consisted of a pond on the tensile face of the beams as shown in Fig. 3.

The corrosion level was estimated using Faraday's law according to Eq. (1).

where t is time (second), i is the current (A), the number 55.847 is Faraday constant (g/mol), and the number 96487 is the molar mass for iron (coulomb).

According to [42], the specimens were immersed in NaCl 5% solution for 48 hours before the direct current was applied.

$$Theoretical\ Mass\ Loss\,(gr) = \frac{t \times i \times 55.847}{2 \times 96487} \quad (1)$$

As shown in Fig. 3, a direct current from the positive terminal of a power supply was impressed onto the ϕ12 reinforcing bars, which in turn flowed to the stainless steel bar (ø8). The applied current eventually reached the negative terminals of the power supply.

To facilitate the corrosion reactions, water was sprayed over the test beams by a fogging compressed air mist nozzle.

The nozzle combines air and water to provide an ultra-fine mist that allows corrosion reactions to occur. The solution of the pond was replaced every 72 hours, and the temperature and moisture of the environment were constant during the test. According to [25], beams were tested while they were under a load equal to 8% of the ultimate load as shown in Fig. 4.

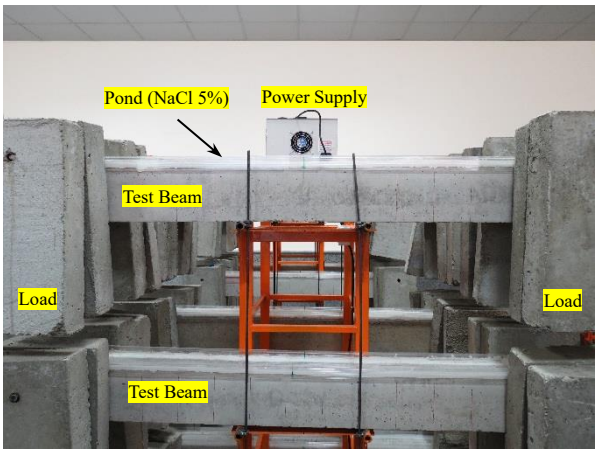

Fig. 4. Test frame for beams under 8% loading and accelerated corrosion.

2.5. Measurement of Half-Cell Potential

The half-cell potentials of reinforcing steels were measured according to ASTM C876 [27] to evaluate the probability of corrosion in RC beams as shown in Fig. 5.

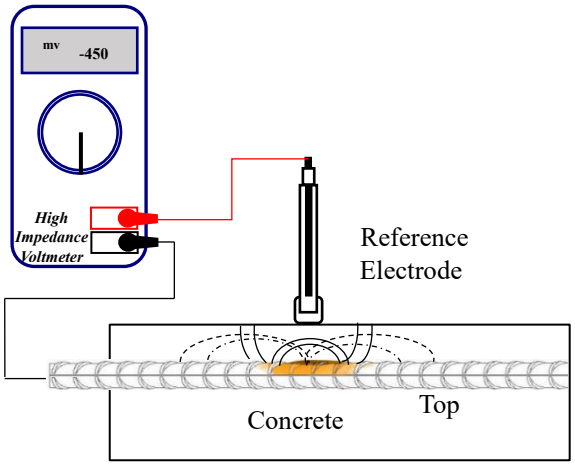

Fig. 5. Schematic illustration of the half-cell potential measurement.

HCP was measured every week at the same time with the same surface moist at different points along the beams length as shown in Fig. 6 (white marks).

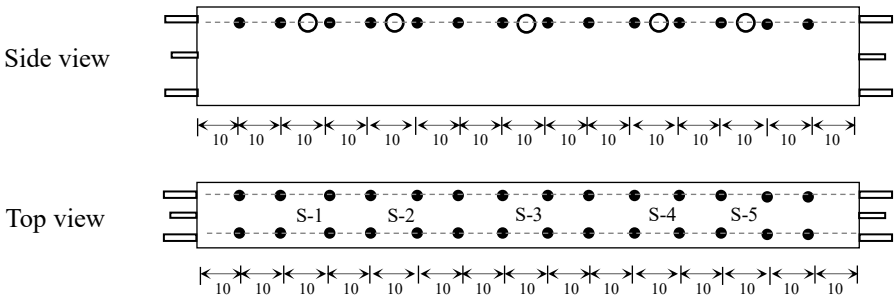

Fig. 6. Typical layout of the tested points along the beam length (All dimensions are in cm).

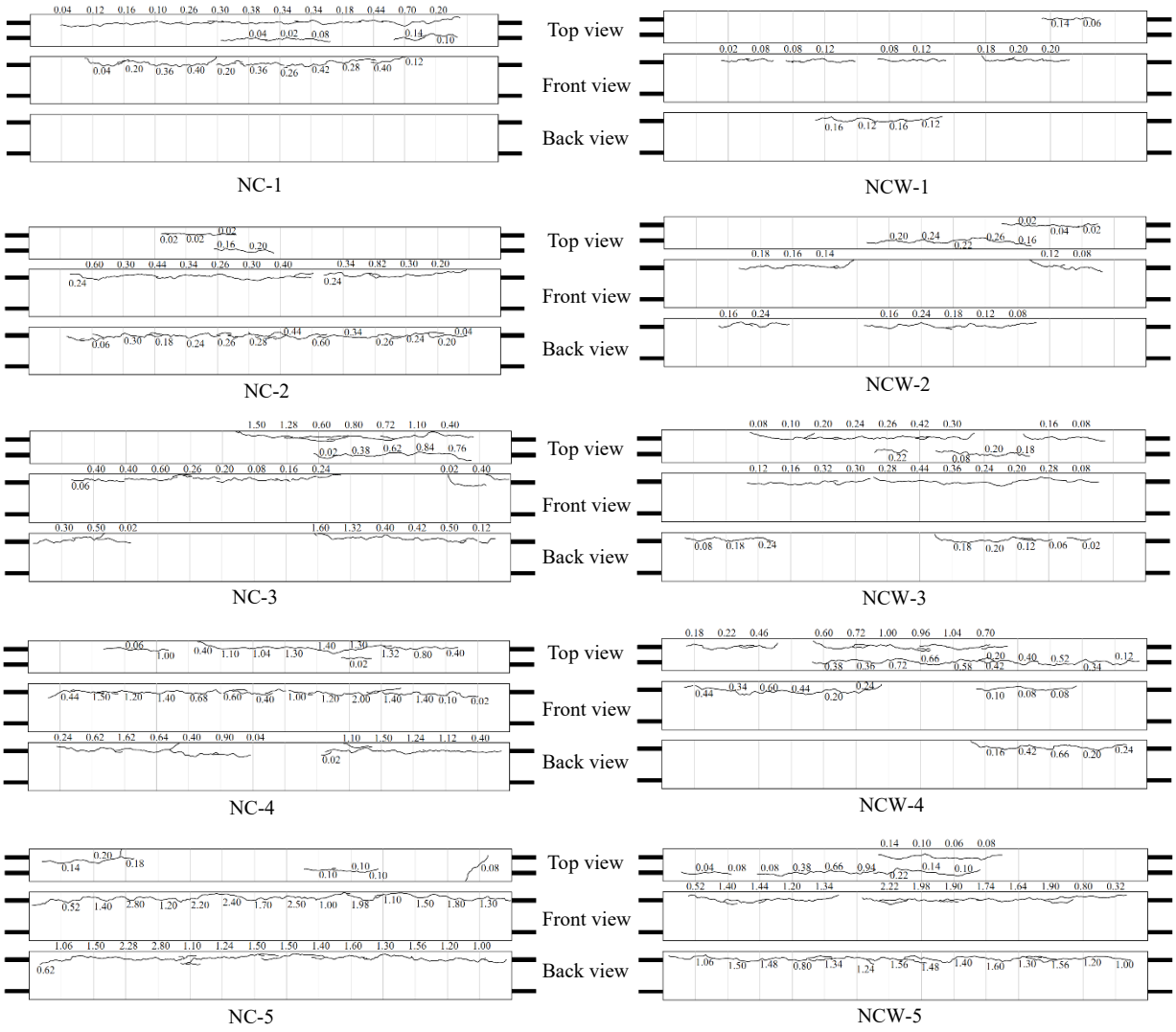

Fig. 7. Corrosion crack patterns for specimens of Groups: (a) NC and (b) NCW.

Positive HCP values indicate a very low corrosion probability, while more negative ones show a higher probability of corrosion activity of the rebars.

2.6. Measurement of Cracks

The corrosion crack width was measured at the end of each period of corrosion exposure

using a hand-held microscope with a magnification of 35X and an accuracy of ±0.02 mm. Corrosion cracks width was measured along the corroded zone of the specimen at 100 mm intervals as shown in Fig. 6 (black marks).

2.7. Measurement of Mass Loss and Rebar Diameter Reduction

At the end of each corrosion phase and after measuring the crack widths, the beams were jackhammered to remove the corroded tensile bars. The rust and all adhered corroded products on the corroded bars were cleaned using a wire brush, and then the bars were soaked in an HCl solution according to ASTM Standards G1-03 method [43]. The clean bars were then weighed and the percentage of mass loss for each bar was calculated based on Eq. (2).

$$\%\,mass\,loss = \frac{(Initial\,weight - Final\,weight)}{Initial\,weight} \times 100 \quad (2)$$

The bar diameter reduction was measured in five different locations along the length of the beam for each tensile bar. These locations are shown in Fig.6 (S-1 to S-5).

3. Results and Discussion

3.1. Crack Patterns and Widths

Corrosion cracks were formed and propagated parallel to the corroding steel bars where expansive corrosion products were drawn into the concrete. The first visible corrosion cracks appeared after approximately 63 and 96 hours for the beams with and without nano wollastonite, respectively.

This result is attributed to a higher density of NCW mixture and therefore it has durability in rebar corrosion resistance. At the end of each corrosion time, the beams were cleaned and the cracking patterns were drawn. The corrosion cracks widths were accurately measured by a hand-held microscope along the length of the beam.

Figs. 7a and b show the schematics of the typical crack patterns after the completion of corrosion duration for NC and NCW beams, respectively. All of the specimens in Groups NC and NCW exhibited corrosion cracks along their length parallel to the tensile steel bars. The average corrosion crack widths measured in the specimens in Group NC were 0.24, 0.30, 0.49, 0.91, and 1.52 mm for NC-1 to NC-5, respectively.

However, these values were 0.07, 0.11, 0.19, 0.5, and 1.35 mm for specimens in Group NCW, from NCW-1 to NCW-5, respectively. The width of corrosion cracks of specimens in Group NCW was less than that of NC Group. Fewer cracks were exhibited in NCW beams in terms of width and number than NC beams at different corrosion levels (low, moderate, and severe). For example, in NC-1 the corrosion cracking area was approximately 665 mm^2, while this amount in NCW-1 was approximately 165 mm^2. Also, the maximum crack widths measured due to corrosion were 0.48, 0.62, 1.60, 1.80, and 2.6mm in the NC-1 to NC-5, respectively. In the NCW-1 to NCW-5, these amounts were 0.20, 0.26, 0.44, 1.04, 2.22 mm, respectively. This result can be attributed to the higher durability of NCW mixture in rebar corrosion resistance, which was due to its dense and enhanced microstructure. As shown in Fig. 8, in a low level of corrosion, the maximum corrosion crack width did not have an obvious relationship with location, and the corrosion cracks width were random.

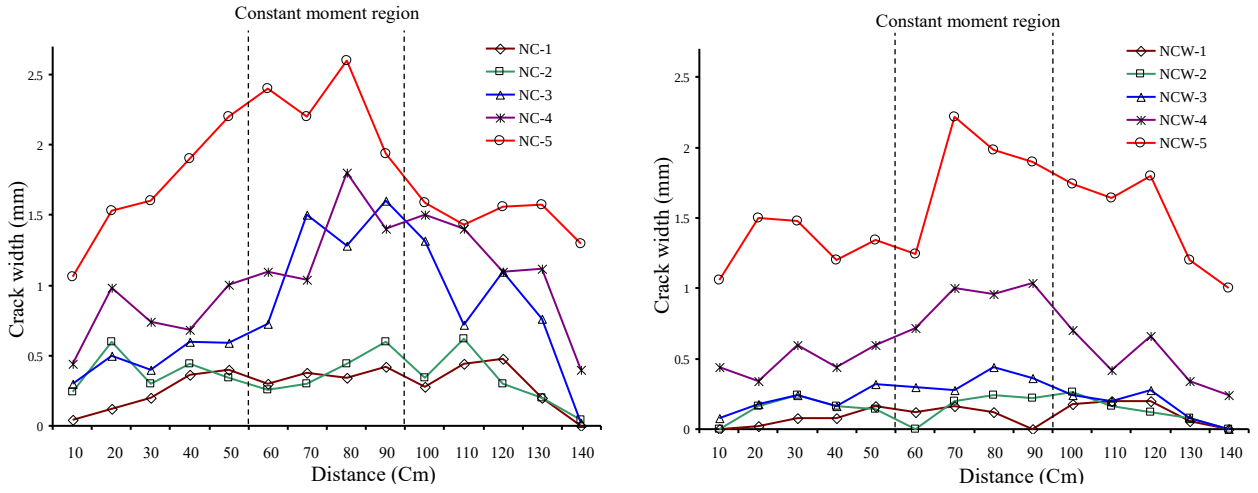

(a) NC beams (b) NCW beams

Fig. 8. Variation of corrosion crack width along the corrosion region at the end of the test.

These results are in agreement with those obtained by Wu et al. [17]. With continuous corrosion process, the maximum crack width appeared in the middle span, in constant moment region. This was more significant in NC-3 in comparison to NCW-3 specimen. As shown in Fig. 8, the trend was observed until the end of the test. The most likely causes of the maximum crack appearance in the middle span are synergistic effects of the stresses of both corrosion products and the bending moment.

To investigate the development of corrosion crack width during the accelerated corrosion process, two specimens, NC-5 and NCW-5, were selected. These beams were corroded up to the end of the last phase of the corrosion exposure (142 days). According to [31], a Demec gauge was used to measure the corrosion crack width. For this purpose, the Demec points were glued to the beam surface perpendicular to the longitudinal axis of the corrosion crack.

The relationship between the corrosion crack width and exposure time for beams NC-5 and NCW-5 is shown in Fig. 9. From this figure, it is evident that corrosion cracks widths in NC-5 specimens were higher compared to those in NCW-5 beams. Incorporation of wollastonite in ultrafine scale into the cement matrix improved mechanical properties and durability of NCW specimens, and therefore the corrosion cracks were decreased.

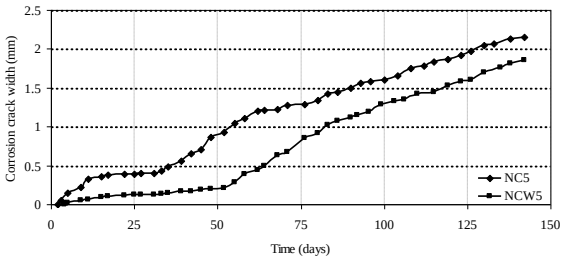

Fig. 9. Corrosion crack width versus time relationship.

For the NC-5, the initial corrosion crack growth rate during the first 15 days of corrosion exposure was approximately 24.0 μm/day.

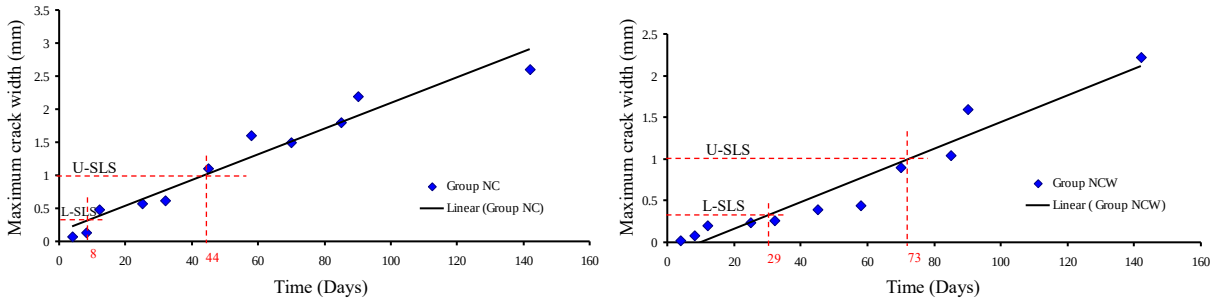

Fig. 10. Width of maximum crack versus time relationship.

Then the growth rate decreased to approximately 8.0μm/day until 35 days of corrosion exposure. This was due to the accumulation of rust layer around the steel bars acting as a barrier against OH^- and Fe^{2+} ions, reducing the corrosion process. After thirty-five days, some micro flexural cracks were probably created, and thus some channels for the ingress of oxygen and moisture became available and consequently the growth rate of corrosion cracks width was increased up to 15.5 μm/day. In the NCW-5 specimen, the initial crack growth rate was approximately 3.8 times less than the rate for the NC-5. This decline can be attributed to the high density of the concrete microstructure due to the use of wollastonite in their mix design. Fig. 9 reveals that there has been a slight rise in the widening of cracks after 15th day until 52th day (≈ 3.10 μm/day). As mentioned in the NC-5 beam, this result is possibly due to the formation of the rust on the tensile steel reinforcing bars. After 52 th day until the end of the test, there was a gradual increase in the corrosion crack growth rate with a speed of 12 μm/day, increasing the interior stress and creating the flexural microcracks, which are important factors in this trending.

Expansive stresses caused by rust formation and flexural tension were the causes of an increase in the corrosion crack growth rate. The rate of corrosion cracks widening was 29% lower in NCW-5 compared to NC-5 specimen in the same duration.As shown in Fig. 9, the average corrosion cracks width in the NC-5 beam was 2.15 mm at the end of corrosion period (142 days). However, this amount in NCW-5 was about 1.85 mm.

An important factor contributing to structural durability is the control of corrosion crack development. The wollastonite could have an important role in increasing the initial cracking time, decreasing the corrosion cracking growth rate, and declining the corrosion crack width. Therefore, it can improve the lifetime of reinforced concrete structures. According to Dura-Crete [44], service limit state (SLS) criteria was achieved when the width of corrosion cracking reached specific values of 0.3 mm (for lower limit L-SLS) or 1.0 mm (for upper limit U-SLS). The values of measured crack width versus the time of corrosion exposure for specimens of groups NC and NCW are shown in Fig. 10.

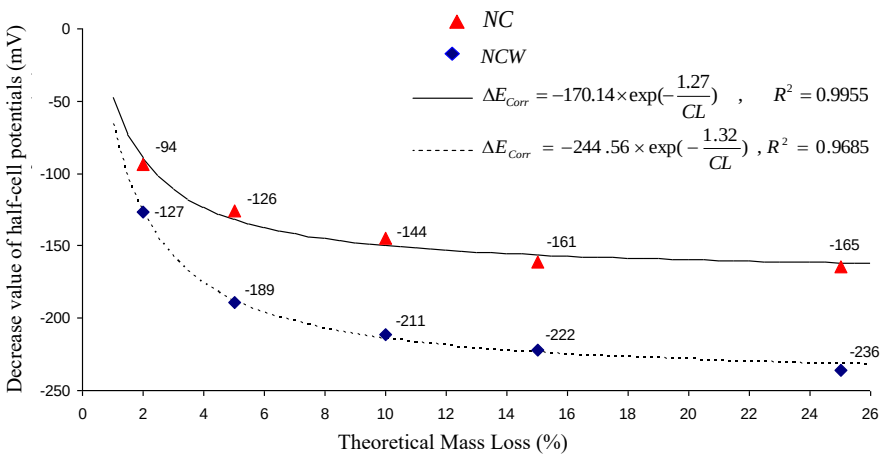

Fig. 11. Decrease value of half-cell potentials versus theoretical mass loss relationship.

In [45], these two criteria were applied to analyze the corrosion results of the beams in the aggressive environment and in the assessment of the lifetime of the reinforced concrete structures.

As can be seen in Fig. 10, the time when a crack with 0.3 mm width (L-SLS) in Group NCW (8 days) appeared was 3.6 times more than that of Group NC (29 days).Based on upper limit criterion proposed by Dura-Crete [44], the service lifetimes of the tested beams were measured, which were 44 and 73 days in NCW and NC groups, respectively. Increasing the time of corrosion cracks with 1.0 mm width, as a limit state life criterion, up to 66% compared to NC beams, could be attributed to concrete durability improvement. Enhancement in durability properties of concrete containing wollastonite was also reported by other researchers [12, 14].

The use of wollastonite as a nanoscale admixture in its mix design was more effective in early age. In other words, the quality of the concrete cover had a key role in the durability of sound concrete. But when corrosion products were formed and cracks were extended, the effect of cover on corrosion process as a hindrance was reduced.

According to this result, the use of L-SLS as a limit state criterion resulted in higher values of lifetime for the reinforced concrete structures compared to the use of U-LSL as a criterion. The observed increase in criterion time could be related to the improvement of the permeability and densification of microstructure in Group NCW. This subject can play a key role in increasing the lifetime of the reinforced concrete structures. Also, by improving the durability of concrete, the cost of repair and maintenance will decrease.

3.2. Half-Cell Potential

The measurements of half-cell potential were done at the beginning and end of the experiment at 5 different locations along the beam length on both sides (Fig. 6).

Average half-cell potential values were calculated for each beam in both Groups NC and NCW. The relationship between half-cell potential and mass loss is shown in Fig. 11. Good correlations can be found between half-cell potential and mass loss, with R^2 values equal to 0.9955 and 0.9685 for NC and NCW respectively.

Table 5. Experimental and theoretical degrees of corrosion.

Group	Specimen	Time of corrosion exposure (Day)	Actual Mass loss (%)		Actual mass loss (Average) (%)	Theoretical mass loss (Faraday's law) (%)	Average crack width (mm)	Maximum crack width (mm)
			Bar 1	Bar 2				
NC	NC-1	12	2.81	2.78	2.80	2.00	0.24	0.48
	NC-2	32	6.40	5.39	5.90	5.00	0.30	0.62
	NC-3	58	7.07	9.95	8.50	10.00	0.49	1.6
	NC-4	85	12.23	15.98	14.10	15.00	0.91	1.8
	NC-5	142	23.75	21.69	22.73	25.00	1.52	2.6
NCW	NCW-1	12	2.74	0.86	1.80	2.00	0.07	0.2
	NCW-2	32	4.85	2.95	3.90	5.00	0.11	0.26
	NCW-3	58	5.54	6.85	6.20	10.00	0.19	0.44
	NCW-4	85	11.32	10.88	11.10	15.00	0.50	1.04
	NCW-5	142	20.40	19.40	19.90	25.00	1.35	2.22

Based on the results shown in Fig. 11, the slope of the curve for NCW beams relative to NC beams is sharper. In other words, in order to achieve the similar mass loss, the half-cell potential reduction values in NCW Group are more than those of NC Group. This result can perhaps be attributed to a higher electrical resistance of NCW mixture, which in turn would result in more positive initial half-cell potential.

3.3. Mass Loss

According to ASTM G1-03 standard [43], the corrosion products adjacent to the tensile bars were removed to obtain the average mass loss. Later the rate of corrosion for each specimen was estimated by both gravimetric method and Faraday's law. The results obtained from these methods are summarized in Table 5.

In Table 5, mass loss of each specimen was calculated by Eq. (2) and the theoretical mass loss was predicted by Faraday's law as shown in Eq. (1). Table 5 shows that the mass loss values, calculated by gravimetric and Faraday's methods were different, in both Group NC and NCW.

It should be noted that the actual mass loss values in the Group NC beams were more than those of Group NCW. The use of nano wollastonite as a partial replacement of cement is a factor in controlling crack development, resulting in the reduction of rebars mass loss. As reported in [2], the Faraday's law has an accurate prediction for the mass loss of a bar suspended in salt solution. But in this study, for the bars embedded in concrete, the mass loss calculated based on Faraday's law was different from the result achieved by gravimetric method.

This discrepancy could be associated with some of the currents which were consumed while passing through the concrete cover. Based on the results presented in Table 5 and Fig. 12, it was also revealed that the actual amount relevant to the theoretical mass loss was higher in NC compared to NCW for all tested beams. Therefore, the proportion of actual to theoretical mass loss values in specimens NC-1, NC-2, NC-3, NC-4, and NC-5 were 1.40, 1.18, 0.85, 0.94, and 0.91, respectively, while in Group NCW, these values were 0.90, 0.78, 0.62, 0.74, and 0.80, respectively.

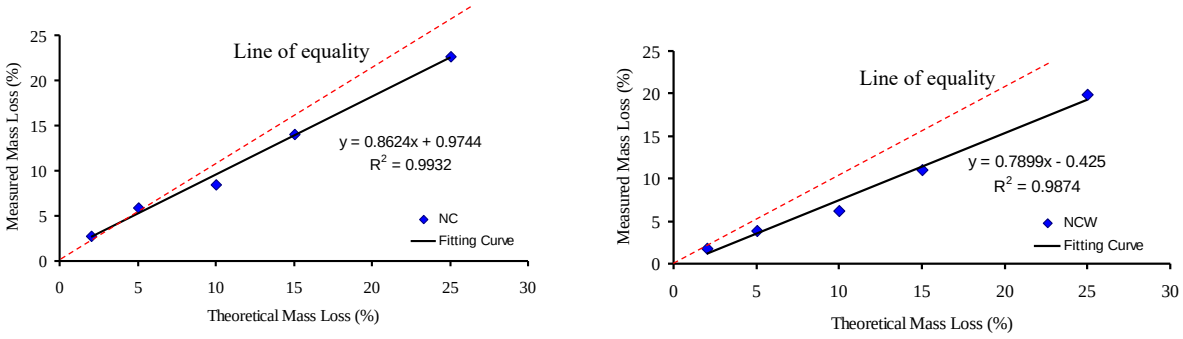

Fig. 12. Comparison of theoretical and measured mass loss in all tested beams.

In NC specimens the corrosion cracks were developed faster than Group NCW. As a result, the concrete resistance decreased rapidly. Accordingly, the achieved mass loss of NC beams was closer to predicted levels. These results are similar to those reported by authors in [2] for SCC concrete beams.

The relationship between measured and theoretical values of mass loss can be expressed for two groups of concrete used in this study as shown in Fig. 12. The linear regression analysis for rebar mass loss between actual and predicted amount due to accelerated corrosion showed good fits (Group NC: R^2 = 0.9932, and Group NCW: R^2 = 0.9874) However, the slopes of the regression analysis line are less than one, so the results of the simulation model are underestimated due to consuming the current passing through the concrete cover that do not contribute to corrosion. This matter is more pronounced in NCW beams. Fig. 13 presents the average crack width and measured rebar mass loss for each group of beams. Fig. 13 indicates the difference between mass loss in NC and NCW specimens where the low level corrosion was higher than high level corrosion.

The measured mass loss amounts for NC-1 and NCW-1 were 60.9 gr and 39.3 gr, respectively, while at the end of the period, these values for NC-5 and NCW-5 were 496.6 gr and 435.6 gr, respectively.

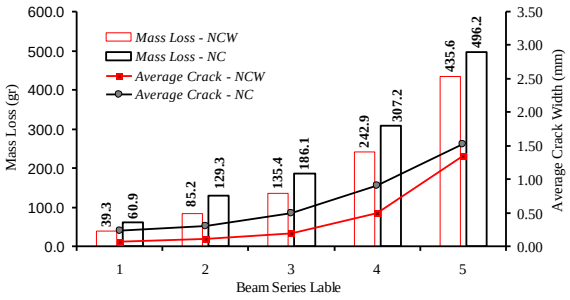

Fig. 13. Evaluation of nano wollastonite influence on mass loss and average crack width at different.

In other words, when the degree of corrosion was lower, the difference between mass loss in NC and NCW specimens reached 35%, while by continuing corrosion process and developing cracks and thereby reducing the electrical resistance, this value decreased and reached a value of 12%.

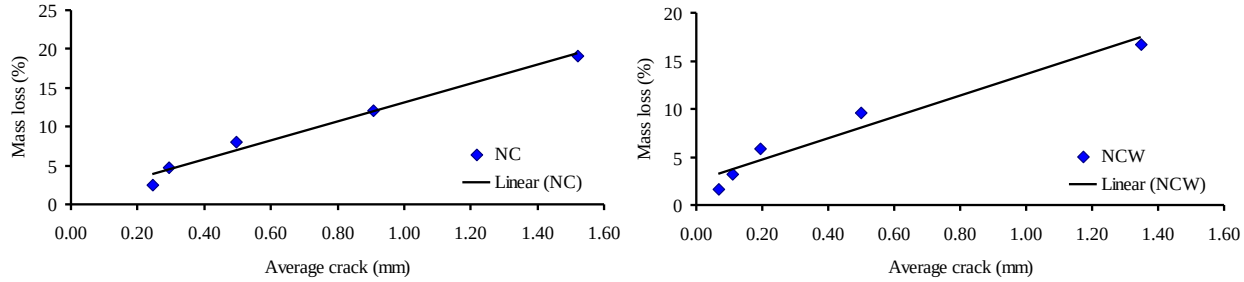

Fig. 14. Mass loss versus average crack width due to corrosion.

Table 6. Results of rebar diameter reduction.

No.	Location	NC Group				NCW Group			
		Crack width (mm)	M/M_{max}	Half-cell reduction (-V)	Diameter reduction (%)	Crack width (mm)	M/M_{max}	Half-cell reduction (-V)	Diameter reduction (%)
1	S-1	0.16	0.25	0.090	1.7	0.05	0.25	0.112	0.6
	S-2	0.38	0.65	0.091	2.1	0.12	0.65	0.113	1.1
	S-3	0.36	1.00	0.090	4.4	0.14	1.00	0.130	2.1
	S-4	0.36	0.65	0.090	2.1	0.19	0.65	0.150	1.0
	S-5	0.34	0.25	0.107	1.1	0.13	0.25	0.128	0.7
2	S-1	0.45	0.25	0.129	3.5	0.2	0.25	0.207	2.4
	S-2	0.39	0.65	0.122	3.8	0.15	0.65	0.193	1.8
	S-3	0.37	1.00	0.133	5.4	0.22	1.00	0.206	3.6
	S-4	0.48	0.65	0.122	1.7	0.21	0.65	0.165	2.1
	S-5	0.25	0.25	0.125	2.2	0.1	0.25	0.176	1.4
3	S-1	0.45	0.25	0.123	4.3	0.21	0.25	0.214	2.5
	S-2	0.6	0.65	0.122	6.7	0.24	0.65	0.198	4.4
	S-3	1.39	1.00	0.176	6.1	0.36	1.00	0.225	4.7
	S-4	1.02	0.65	0.183	3.8	0.22	0.65	0.222	3.5
	S-5	0.93	0.25	0.118	2.5	0.18	0.25	0.196	2.6
4	S-1	0.86	0.25	0.142	5.7	0.47	0.25	0.228	5.0
	S-2	0.844	0.65	0.204	8.5	0.52	0.65	0.180	5.4
	S-3	1.42	1.00	0.200	9.3	0.98	1.00	0.257	7.1
	S-4	1.45	0.65	0.162	9.2	0.56	0.65	0.239	6.9
	S-5	1.11	0.25	0.098	7.7	0.5	0.25	0.208	5.9
5	S-1	1.56	0.25	0.173	7.4	1.49	0.25	0.285	7.5
	S-2	2.05	0.65	0.147	14.3	1.27	0.65	0.216	8.7
	S-3	2.4	1.00	0.202	20.2	2.1	1.00	0.288	14.3
	S-4	1.51	0.65	0.175	6.0	1.69	0.65	0.218	11.9
	S-5	1.56	0.25	0.126	8.1	1.5	0.25	0.171	6.4

Also, as can be seen in Fig. 13, by continuing the accelerated corrosion process, the corrosion-induced cracks width increased. As a result, concrete permeability increased and the influence of wollastonite on corrosion rate decreased. Therefore, the difference between mass loss in NC and NCW specimens in high levels of corrosion declined.

Moreover, in both Groups NC and NCW, the mass loss of reinforcing steel due to

corrosion can be determined by the following equations based on Fig. 14:

It has to be noted that linear relationship between rebar mass loss and average corrosion crack width may be considered for design purposes.

In Group NC:

$$Mass\,loss(\%) = 12.191 \times (Average\ crack) + 0.9339, \quad R^2 = 0.9807 \qquad (3)$$

In Group NCW:

$$Mass\,loss(\%) = 11.013 \times (Average\ crack) - 2.5724, \quad R^2 = 0.9510 \qquad (4)$$

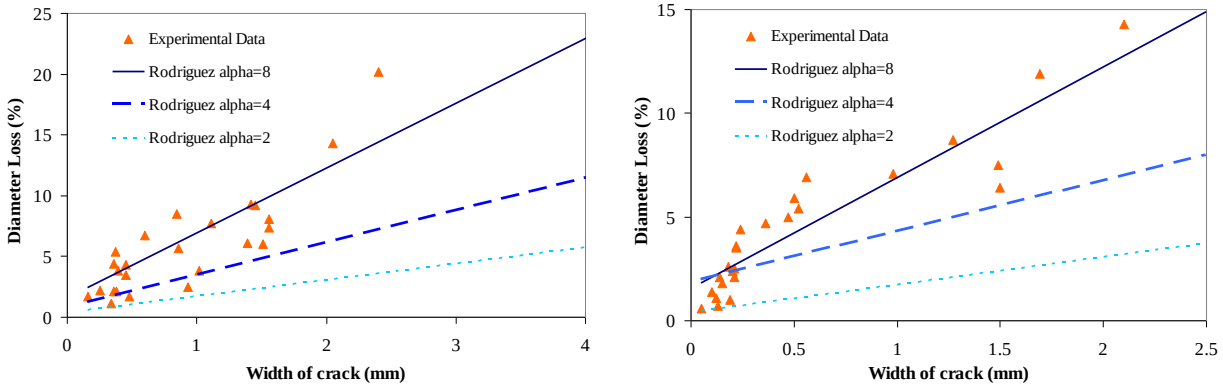

(a) NC beams (b) NCW beams

Fig. 15. Comparison of experimental data with Rodriguez et al.'s model.

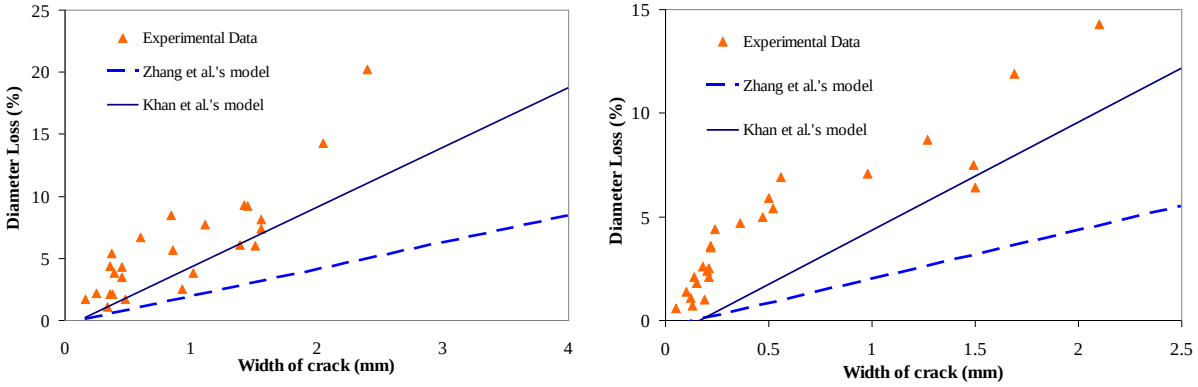

(a) NC beams (b) NCW beams

Fig. 16. Comparison of experimental data with Zhang et al.'s and Khan et al.'s models.

3.4. Rebar Diameter Reduction

Average rebars diameter reduction, half-cell potential reduction, and corrosion crack width; measured at 5 different locations along the beam length in both Group NC and NCW are summarized in Table 6.

It can be seen from the data in Table 6 that by increasing the corrosion crack width, the value of the rebar diameter reduction increased, too. Moreover, the ratio of existing moment to maximum moment was significantly effective in diameter degradation. In NCW Group, rebar diameter reduction was less than that of NC Group at the same time. This result can perhaps be attributed to a higher density and more electrical resistance of NCW mixture. In order to analyze the relationship between crack width and steel cross-section loss, the results obtained in this study were compared with the models established by Rodriguez et al. [19], Zhang et al. [21] and Khan et al.[22].

Figs. 15a and b show a comparison of Rodriguez et al.'s model [19] with the experimental results for NC and NCW beams, respectively. In Rodriguez et al.'s model, the value of crack penetration factor, α, depends on corrosion type [22].

It can be seen that, for a value of $\alpha = 2$, in both NC and NCW beams, the model significantly overestimates the steel cross-section loss. In NC beams with normal concrete (Fig. 15a), and the value of $4 < \alpha < 8$, the relationship between the model and the experimental results seems to be good. For the smaller experimental values of crack width, a value of $\alpha = 4$ used in the model gave satisfactory results, but for the larger experimental values of corrosion crack width in the maximum moment region, the value of $\alpha = 8$ used in the model was more accurate in predicting the loss of steel cross- section. As shown in Fig. 15b, in NCW beams Rodriguez et al.'s model is not in relation with experimental data. The amount of this difference is higher in lower corrosion rates for different values of α. Thus it can be seen that it is difficult to decide the value of α which is used for the model in different conditions. Choosing an incorrect value of crack penetration factor, α, can lead to overestimated or under-estimated values for the loss of steel cross-section for a given crack width. Using the traditional modeling techniques like Rodriguez et al.'s model, to predict the rebar diameter reduction values is unreliable.

In addition, Figs. 16a and b provide the comparison of experimental results with Zhang et al's [21] and Khan et al.'s [22] models for NC and NCW beams, respectively. As shown in these figures, the Khan's results (modified Zhang model) are in close agreement with the experimental results, while the predictions of Zhang et al.'s model are much underestimated. This result is close to the findings of ref. [22].

However, both models lead to overestimated values for the loss of steel cross-section for a given crack width. This discrepancy may be explained by the fact that the synergistic effect of simultaneous sustained loading and corrosion is ignored, especially in corrosion propagation levels.

In this paper, to overcome the limitations of the existing models, GMDH-type neural network is used in modeling of rebar diameter reduction (f) in reinforced concrete beams according to input parameters. These include corrosion crack width (X_1), ratio moment value (X_2), and decrease value of the half-cell potential (X_3).

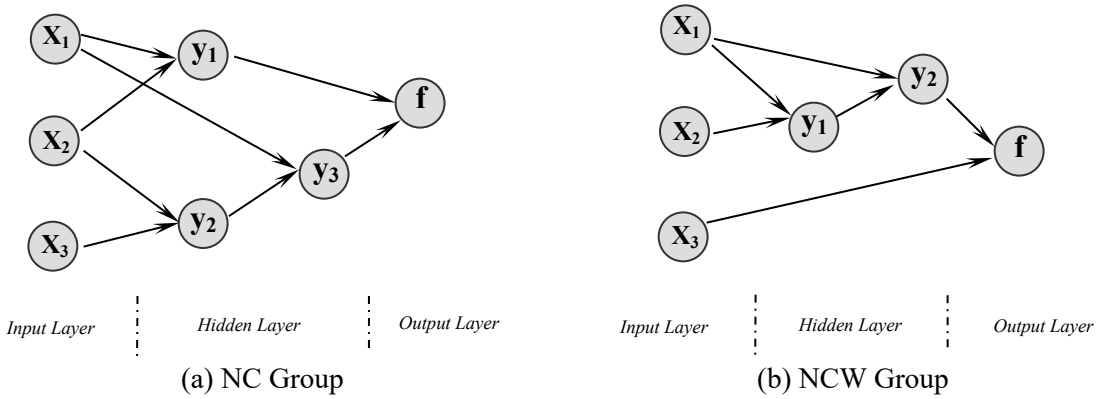

Fig. 17. Evolved structure of generalized GMDH-type neural network model.

3.4.1. GMDH Modeling

According to [29], the GMDH-type neural networks are used to find the polynomial model of rebar diameter reduction in respect to its effective input parameters in both NC and NCW Groups. In order to genetically design such GMDH-type neural network, a population of 50 individuals with a crossover probability of 0.75 and mutation probability of 0.07 were used in 300 generations. The structure of the evolved 3-hidden layer GMDH-type neural network is shown in Fig. 17. The corresponding polynomial representation of models for rebar diameter reduction in NC and NCW Groups are as follows:

$$\begin{aligned}
Y_1 &= 2.55434 - 1.76055 \times (X_1) - 0.09352 \times (X_2) + 3.45479 \times (X_1)^2 + 2.22374 \times (X_2)^2 - 0.34715 \times (X_1) \times (X_2) \\
Y_2 &= 0.33356 + 37.59473 \times (X_3) - 10.39428 \times (X_2) + 1.15178 \times (X_3)^2 + 5.93089 \times (X_2)^2 + 44.62169 \times (X_3) \times (X_2) \\
Y_3 &= 2.39263 + 0.37392 \times (Y_2) - 4.25788 \times (X_1) + 0.06439 \times (Y_2)^2 + 6.19443 \times (X_1)^2 - 0.78119 \times (Y_2) \times (X_1) \\
f &= 0.16327 + 0.23904 \times (Y_1) + 0.57564 \times (Y_3) + 0.52499 \times (Y_1)^2 + 0.52744 \times (Y_3)^2 - 1.04152 \times (Y_1) \times (Y_3)
\end{aligned} \tag{5}$$

$$\begin{aligned}
Y_1 &= 0.19962 + 6.62939 \times (X_1) + 3.59801 \times (X_2) - 2.18428 \times (X_1)^2 - 3.42900 \times (X_2)^2 + 4.36955 \times (X_1) \times (X_2) \\
Y_2 &= -2.70513 - 9.92157 \times (X_1) + 3.53548 \times (Y_1) - 17.97337 \times (X_1)^2 - 0.67880 \times (Y_1)^2 + 6.79683 \times (X_1) \times (Y_1) \\
f &= -3.53346 + 40.01823 \times (X_3) + 0.43284 \times (Y_2) - 99.20427 \times (X_3)^2 + -0.00746 \times (Y_2)^2 + 2.54460 \times (X_3) \times (Y_2)
\end{aligned} \tag{6}$$

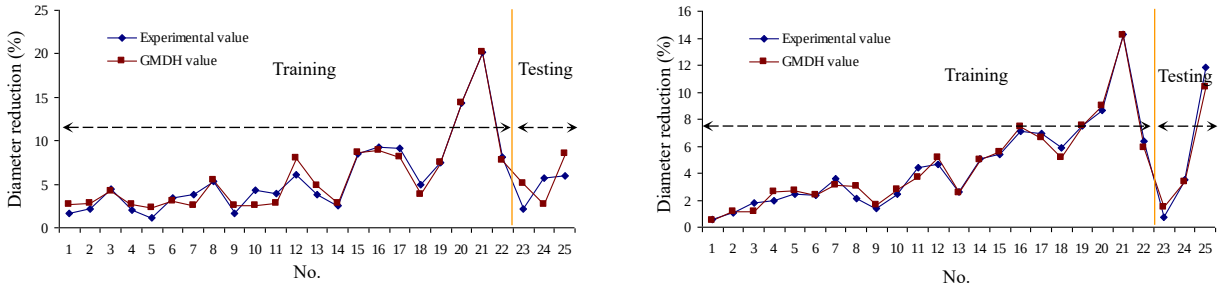

Fig. 18. Comparison between experimental values and results of evolved GMDH-type neural network model (training and testing).

In Fig. 18, the very good behavior of the GMDH-type neural network models for training and testing data of compressive strength of mortar is depicted. It is evident that in terms of simple polynomial equations, the evolved GMDH-type neural network

could successfully model and predict the output of testing data, which were not used during the training process.

4. Conclusion

The present study was designed to determine the effect of nano wollastonite on cracking behavior of reinforced concrete beams caused by corrosion in comparison with normal concrete under the accelerated corrosion condition. The study evaluated the corrosion crack patterns, crack widths, and mass loss of rebar due to corrosion at different levels. One of the most significant findings which emerged from this study was that incorporation of nano wollastonite in concrete beams improved concrete's durability and reduced its growth rate of corrosion cracks width. As a result, according to limit criteria proposed by Dura-Crete [44], the use of nano wollastonite as a partial replacement of cement can increase the service life of reinforced concrete structures. Moreover, the following conclusions can be drawn from the present study:

- Incorporation of nano wollastonite into the concrete could have an important role in improving the mechanical properties and durability of reinforced concrete structures by increasing the initial cracking time and decreasing the corrosion induced crack growth rate and rebar mass loss.
- As a result of the use of wollastonite in concrete, the emerging time of the first visible corrosion crack in NCW specimens was 1.52 times more than that of NC specimens.
- At different corrosion levels, NCW specimens exhibited fewer cracks in terms of width and number than NC beams. Therefore, in specimens with a low level of corrosion, NC-1 and NCW-1, the cracking areas were approximately 665 mm^2 and 165 mm^2, respectively.
- Due to synergistic effects of corrosion products stresses and the flexural stress, which was due to sustained load, the maximum corrosion crack width appeared in the middle span after moderate corrosion (after 58 days).
- In NCW beams, the initial crack growth rate was approximately 3.8 times less than the rate for the NC beams. With continuous corrosion process, this value declined and reached 1.29.
- By considering L-SLS and U-SLS as limit state criteria, the lifetime of the NCW specimens was 3.6 and 1.66 times longer than that of Group NC, respectively.
- When the degree of corrosion was on a lower level, the difference between mass loss in NC and NCW specimens reached 35%, while by continuing corrosion process and development of cracks and thereby reducing the electrical resistance, this value decreased and reached 12%.
- In NCW specimens, due to consuming the current in order to pass through the durable concrete cover, measured rebar mass loss by gravimetric method was on average 23% less than that predicted by Faraday's Law.
- The obtained linear relationship between the average corrosion crack width and rebar mass loss can be used for design purposes in the aggressive environment.
- The experimental results agreed with Rodriguez et al.'s model when the value of the corrosion penetration factor, α, was between 4 and 8. However, it was difficult to decide the value of α which was needed. Also, Predictions from Zhang et al.'s and Khan et al.'s models

were considerably lower than the experimental values obtained in this study.

- GS-GMDH neural network is an effective tool for modeling and predicting the rebar diameter reduction in aggressive environments.

More research is required in order to determine the long-term corrosion parameters in reinforced concrete beams containing nano wollastonite in the natural corrosive environment. However, by replacing the part of the cement with nano wollastonite, as a mineral admixture with a low cost and large reserve in the world, environmental pollution, greenhouse gases, energy demands, and high production cost will significantly decrease.

REFERENCES

[1] Zou, Z. H., Wu, J., Wang, Z., Wang, Z. (2016). "Relationship Between Half-Cell Potential and Corrosion Level of Rebar in Concrete, Corrosion Engineering." Science and Technology, Vol. 51, Issue 8, pp. 588-595.

[2] Hassan, A. A. A., Hossain, K. M. A., Lachemi, M. (2009). "Corrosion Resistance of Self-Consolidating Concrete in Full-Scale Reinforced Beams. " Cement and Concrete Composites, Vol. 31, Issue 1, pp. 29-38.

[3] Aveldaño, R. R., Ortega, N. F. (2011). "Characterization of concrete cracking due to corrosion of reinforcements in different environments." Construction and Building Materials, Vol. 25, Issue 2, pp. 630-637.

[4] Malumbela, G. (2010). "Measurable Parameters for Performance of Corroded and Repaired RC Beams Under Load." Phd thesis, Department of Civil Engineering, University of Cape Town, South Africa.

[5] Supit, S., Shaikh, F. U. A. (2015). "Durability Properties of High Volume Fly Ash Concrete Containing Nano Silica." Materials and Structures, Vol. 48, Issue 8, pp. 2431-2445.

[6] Shaikh, F. U. A., Supit, S. W. M. (2015). "Chloride Induced Corrosion Durability of High Volume Fly Ash Concretes Containing Nano Particles." Construction and Building Materials, Vol. 99, pp. 208-225.

[7] Ranjbar, M. M., Madandoust, R., Mousavi, S. Y., Yosefi, S. (2013). "Effects of Natural Zeolite on the Fresh and Hardened Properties of Self-Compacted Concrete." Construction and Building Materials, Vol. 47, pp. 806-813.

[8] Torkaman, J., Ashori, A., Sadr Momtazi, A. (2014). "Using Wood Fiber Waste, Rice Husk Ash, and Limestone Powder Waste as Cement Replacement Materials for Lightweight Concrete Blocks." Construction and Building Materials, Vol. 50, pp. 432-436.

[9] Kalla, P., Misra, A., Gupta, R. C., Csetenyi, L., Gahlot, V. (2013). "Mechanical and Durability Studies on Concrete Containing Wollastonite–Fly ash Combination." Construction and Building Materials, Vol. 40, pp. 1142-1150.

[10] Sujjavanich, S., Suwanvitaya, P., Chaysuwan, D., Heness, G. (2017). "Synergistic Effect of Metakaolin and Fly ash on Properties of Concrete." Construction and Building Materials, Vol. 155, pp. 830–837.

[11] Al Menhosh, A., Wang, Y., Wang, Y., Augusthus-Nelson, L. (2018). "Long Term Durability Properties of Concrete Modified with Metakaolin and Polymer Admixture." Construction and Building Materials, Vol. 172, pp. 41–51

[12] Miri, M., Beheshti Nezhad, H., Jafari, M. (2014). "Experimental Investigation on Mechanical Properties of Concrete Containing Nano Wollastonite and Modeling with GMDH- Type Neural Networks." (in Persian), Amirkabir Journal of Science & Research (Civil & Environmental Engineering), Vol. 46, Issue 2, pp. 49- 51.

[13] Ni, T., Zhang, L., Yuan, B. (2011). "Influence of Wollastonite or Plant Fiber on Performance of Autoclaved Cement Concrete." Applied Mechanics and Materials, Vol. 99-100, pp. 692-695.

[14] Kalla, P., Rana, A., Chad, Y. B., Misra, A., Csetenyi, L. (2015). "Durability Studies on Concrete Containing Wollastonite." Journal of Cleaner Production, Vol. 87, pp. 726-734.

[15] Soliman, A. M., Nehdi, M. L. (2014). "Effects of Shrinkage Reducing Admixture and Wollastonite Microfiber on Early-Age Behavior of Ultra-High Performance Concrete." Cement and Concrete Composites, Vol. 46, pp. 81-89.

[16] Zhang, L. C. (2013). "Durability of Concrete Containing Wollastonite and Fly Ash." Advanced Materials Research, Vol. 800, pp. 361-364.

[17] Wu, F., Gong, J. h., Zhang, Z. (2014). "Calculation of Corrosion Rate for Reinforced Concrete Beams Based on Corrosive Crack Width." Journal of Zhejiang University SCIENCE A, Vol. 15, Issue 3, pp. 197-207.

[18] Cao, Ch., Cheung, M.M.S., Chan, B.Y.B. (2013). "Modelling of Interaction Between Corrosion-Induced Concrete Cover Crack and Steel Corrosion Rate." Corrosion Science, Vol. 69, pp. 97–109

[19] Rodriguez, J., Ortega, L.M., Casal, J., Diez, J.M. (1996). "Corrosion of Reinforcement and Service Life of Concrete Structures." Durability of Building Materials and Components, Vol. 7, Issue 1, pp. 117–126.

[20] Vidal, T., Castel, A., François, R. (2004). "Analyzing Crack Width to Predict Corrosion in Reinforced Concrete." Cement and Concrete Research, Vol. 34, pp. 165–174.

[21] Zhang, R., Castel, A., François, R. (2010). "Concrete Cover Cracking with Reinforcement Corrosion of RC beam During Chloride-Induced Corrosion Process." Cement and Concrete Research, Vol. 40, pp. 415–425.

[22] Khan, I., François, R., Castel, A. (2014). "Prediction of Reinforcement Corrosion Using Corrosion Induced Cracks Width in Corroded Reinforced Concrete Beams." Cement and Concrete Research, Vol. 56, pp. 84–96

[23] Li, H., Li, B., Jin, R., Li, Sh., Yu, J-G. (2018). "Effects of Sustained Loading and Corrosion on the Performance of Reinforced Concrete Beams." Construction and Building Materials, Vol. 169, pp. 179–187.

[24] Ye, H., Fu, Ch., Jin, N., Jin, X. (2018). "Performance of Reinforced Concrete Beams Corroded under Sustained Service Loads: A Comparative Study of Two Accelerated Corrosion Techniques." Construction and Building Materials, Vol. 162, pp. 286–297.

[25] Malumbela, G., Moyo, P., Alexander, M. (2012). "Longitudinal Strains and Stiffness of RC Beams under Load as Measures of Corrosion Levels." Engineering Structures, Vol. 35, pp. 215-227.

[26] Kim, Y. Y., Kim, J. M., Bang, J.-W., Kwon, S.-J. (2014). "Effect of Cover Depth, W/C Ratio, and Crack Width on Half Cell Potential in Cracked Concrete Exposed to Salt Sprayed Condition." Construction and Building Materials, Vol. 54, pp. 636-645.

[27] ASTM C 876. (2015). "Standard Test Method for Half Cell Potential of Reinforcing Steel in Concrete." West Conshohocken, PA: ASTM International.

[28] Nygaard, P. V. (2008). "Non-Destructive Electrochemical Monitoring of Reinforcement Corrosion." Phd thesis, Department of Civil Engineering, Technical University of Denmark.

[29] Madandoust, R., Bungey, J. H., Ghavidel, R. (2012). "Prediction of the Concrete Compressive Strength by Means of Core Testing Using GMDH-Type Neural Network and ANFIS Models." Computational Materials Science, Vol. 51, pp. 261–272.

[30] Du, Y., Cullen, M., Li, C. (2013). "Structural Performance of RC Beams under Simultaneous Loading and Reinforcement Corrosion." Construction

and Building Materials, Vol. 38, pp. 472–481.

[31] El Maaddawy, T., Soudki, Kh., Topper, T. (2005). "Long-Term Performance of Corrosion-Damaged Reinforced Concrete Beams." ACI Structural Journal, Vol. 102, Issue 5, pp. 649-656.

[32] ASTM C150. (2009). "Standard Specification for Portland Cement." West Conshohocken, PA: ASTM International.

[33] Balaguru, P., Chong, K. (2008). "Nanotechnology and Concrete: Research Opportunities." In Nanotechnology of concrete: Recent Developments and Future Perspectives (ACI SP-254), Detroit, MI: American Concrete Institute.

[34] Sanchez, F., Sobolev, K. (2010). "Nanotechnology in Concrete – a Review." Construction and Building Materials, Vol. 24, pp. 2060–2071.

[35] ASTM C 618. (2015). "Standard Specification for Coal Fly Ash and Raw or Calcined Natural Pozzolan for Use in Concrete." West Conshohocken, PA: ASTM International.

[36] ASTM C33. (2016). "Standard Specification for Concrete Aggregates." West Conshohocken, PA: ASTM International.

[37] ASTM C494/C494M-10. (2010). "Standard Specification for Chemical Admixtures for Concrete." West Conshohocken, PA: ASTM International.

[38] ASTM C 143. (2001). "Standard Test Method for Slump of Hydraulic-Cement Concrete." West Conshohocken, PA: ASTM International.

[39] BS 1881: Part 116. (1983). "Testing Concrete: Method for Determination of Compressive Strength of Concrete Cubes." British Standard Institution (BSI).

[40] El Maaddawy, T., Soudki, Kh. (2003). "Effectiveness of Impressed Current Technique to Simulate Corrosion of Steel Reinforcement in Concrete." Journal of Material in Civil Engineering, Vol. 15, Issue 1, pp. 41-47.

[41] Malumbela, G., Moyo, P., Alexander, M. (2012). "A Step Towards Standardising Accelerated Corrosion Tests on Laboratory Reinforced Concrete Specimens." Journal of the South African institution of civil engineering, Vol. 54, Issue 2, pp. 78–85.

[42] Rinaldi, Z., Imperatore, S., Valente, C. (2010). "Experimental Evaluation of the Flexural Behavior of Corroded P/C Beams." Construction and Building Materials, Vol. 24, pp. 2267–2278.

[43] ASTM G1. (2003). "Standard Practice for Preparing, Cleaning, and Evaluating Corrosion Test Specimens." West Conshohocken, PA: ASTM International.

[44] DuraCrete-Final Technical Report. (2000). "The European Union-Brite EuRam III Research Project: Probabilistic Performance Based Durability Design of Concrete Structures." Document BE95-1347/R17, CUR, Gauda.

[45] Zhang, R., Castel, A., Francois, R. (2009). "Serviceability Limit State Criteria Based on Steel–Concrete Bond Loss for Corroded Reinforced Concrete in Chloride Environment." Materials and Structures, Vol. 42, pp. 1407–1421.